Check for updates

Analytical Methods Hot Paper

How to cite: *Angew. Chem. Int. Ed.* **2022,** *61,* e202115907
International Edition: doi.org/10.1002/anie.202115907
German Edition: doi.org/10.1002/ange.202115907

CLIPON: A CRISPR-Enabled Strategy that Turns Commercial Pregnancy Test Strips into General Point-of-Need Test Devices

Yidan Tang, Lijuan Qi, Yichen Liu, Lulu Guo, Rujian Zhao, Meiting Yang, Yan Du, and Bingling Li**

Abstract: *Desirable biosensing assays need to be sensitive, specific, cost-effective, instrument-free, and versatile. Herein we report a new strategy termed CLIPON (CRISPR and Large DNA assembly Induced Pregnancy strips for signal-ON detection) that can deliver these traits. CLIPON integrates a commercial pregnancy test strip (PTS) with four biological elements: the human chorionic gonadotropin (hCG), CRISPR-Cas12a, crRNA and cauliflower-like large-sized DNA assemblies (CLD). CLIPON uses the Cas12a/crRNA complex both to recognize a target of interest and to release CLD-bound hCG so that target presence can translate into a colorimetric signal on the PTS. We demonstrate the versatility of CLIPON through sensitive and specific detection of HPV genomic DNA, SARS-CoV-2 genomic RNA and adenosine. We also engineer a cell phone app and a hand-held microchip to achieve signal quantification. CLIPON represents an attractive option for biosensing and point-of-care diagnostics.*

Introduction

Simple and portable point-of-care testing (POCT) that can be carried out at resource-limited locations, or point of need in general, is of vital importance in disease control, food safety and environmental monitoring. However, there is very limited availability of simple and portable POCT devices that are highly effective to meet the need by both skilled professionals and the general public. This is evident during the on-going COVID-19 pandemic, as the most reliable detection of SARS-CoV-2 viruses is still done with RT-PCR, which requires sophisticated instrumentation and thus restricted to clinical diagnostic laboratories staffed with skilled technicians. Very few portable POCT options suitable for unsupervised self-testing are available, even though there are huge demands for such tests. There isn't a lack of excellent ideas that have great potential for creating novel and effective POCT devices; however, it takes considerable time to translate these ideas into commercially viable devices, and therefore, these elegant ideas may not make an immediate impact at the time of need. One strategy that can significantly shorten the idea-to-market time is repurposing existing POCT devices for the detection of the targets that these devices are not originally designed for,[1–3] simply because such a strategy avoids the most time-consuming processes required for device design, optimization and fabrication. The first example of this concept was the use of personal glucose meter for the detection of nucleic acids,[3–6] which uses chemical reactions to link the presence of a nucleic acid target to the generation of glucose. An even simpler example is the reuse of pregnancy test strip (PTS, a lateral flow test strip) for a different purpose: PTS is designed to detect the human chorionic gonadotropin (hCG), a hormone associated with pregnancy; however, we and others have repurposed PTS for the detection of other types of targets, such as DNA and RNA. This is done through translating the presence of the target of interest to the generation of hCG, so that the detection of this target can be simply done with PTS devices that are commercially available at very low price.[7–10]

However, there are still significant challenges in adopting existing POCT devices for the detection of different targets, which often make the repurposed applications less practical or user-friendly. For example, repurposing PTS for the detection of DNA commonly requires covalent coupling of hCG to a single-stranded (ss) DNA (ssDNA) molecule, forming a ss nucleic acid (ssDNA)-hCG conjugation probe (NHP) as the intermediate probe to transduce target-probe binding to a PTS signal. In the published strategies,[7–10] the NHP has to be hybridized to a partially complementary DNA strand pre-immobilized on large-sized substrates (e.g., magnetic microbeads or water-soluble nucleic acid microflowers) to make it unavailable for strip migration and signal generation. The detection of the target DNA of interest is achieved via a sequence-specific strand-displacement reaction that releases the NHP from the substrate so that the hCG-containing NHP can now migrate on PTS to produce a colorimetric readout. Even with considerable advancement, such a transduction strategy has shown multiple practical problems. First, it needs complicated substrate preparation or heterogeneous washing and separating steps which may affect the signal stability and operational flexibility. Second, since the read-out signal highly depends on the 1:1 strand-displacement between the DNA target and the NHP, one target molecule can only free one NHP, which often results in poor detection sensitivity. Third, even though the system

[*] Dr. Y. Tang, L. Qi, Y. Liu, L. Guo, R. Zhao, Dr. M. Yang, Prof. Y. Du, Prof. B. Li
State Key Lab of Electroanalytical Chemistry, Changchun Institute of Applied Chemistry, Chinese Academy of Sciences, Changchun, Jilin, 130022 (P. R. China)
E-mail: duyan@ciac.ac.cn
binglingli@ciac.ac.cn
L. Qi, Y. Liu, L. Guo, R. Zhao, Prof. Y. Du, Prof. B. Li
University of Science and Technology of China, Hefei, Anhui 230026 (P. R. China)

© 2022 Wiley-VCH GmbH

15213773, 2022, 12, Downloaded from https://onlinelibrary.wiley.com/doi/10.1002/anie.202115907 by Shanghai Normal University, Wiley Online Library on [05/02/2023]. See the Terms and Conditions (https://onlinelibrary.wiley.com/terms-and-conditions) on Wiley Online Library for rules of use; OA articles are governed by the applicable Creative Commons License

works well for the detection of ss nucleic acid species, it is not easy to expand the design for detection of double-stranded (ds) DNA (dsDNA) or non-nucleic acid targets. Finally, whenever a new DNA sequence needs to be detected, the strand displacement reaction has to be redesigned, which includes building a new set of sequences for strand displacement and re-synthesizing a new NHP for signal transduction, adding the time, cost and risk for failure. Such issues are common for POCT repurposing and overcoming them represents the most important next step in this research space.

Herein, we provide a comprehensive solution to above issues through the development of a new concept which we term CLIPON (CRISPR and Large DNA assembly Induced Pregnancy strips for signal-ON detection). CLIPON integrates four components: NHP, CRISPR-Cas12a, a CRISPR RNA (crRNA) and cauliflower-like large-sized DNA assemblies (CLD) formed by stem-loop concatamers. It works by the mechanism illustrated in Figure 1, which uses the detection of a double-stranded DNA target as an example. First, the crRNA is designed to be complementary to part of the DNA target so that the crRNA/CRISPR-Cas12a complex will specifically recognize the target of interest. Second, binding between the crRNA/CRISPR-Cas12a complex and the DNA target activates the non-specific DNA cleavage activity of Cas12a.[11,12] Third, the activated Cas12a then cleaves the DNA tag of NHP. Finally, CLD is designed to hybridize with the DNA tag within NHP to prevent NHP from migrating on PTS to generate a signal; however, with the removal of the DNA tag by the target-induced cleavage, the hCG component of NHP can no longer hybridize with CLD, and therefore, the digested NHP is able to migrate on PTS. The outcome of the entire process is the generation of both a test line and a control line on PTS when the DNA target is present, but only a control line when the DNA target is absent, achieving the signal-ON detection of the target. CLIPON offers three features that are unmatched by published PTS methods. First, previous methods have all used strand displacement for target recognition and CLIPON uses CRISPR-Cas12a mediated DNA recognition to activate the trans DNA cleavage activity of CRISPR,[11–17] which offers higher recognition specificity and enzymatic turnover to amplify the recognition event. Second, previous methods can only directly detect ss nucleic acid targets, while CLIPON can detect nucleic acids both in ss and ds forms. Given biological DNA molecules almost exclusively exist in ds form, CLIPON can be used for biological DNA detection without the need of incorporating strategies to convert dsDNA into ssDNA. Third, the DNA tag in NHP is completely independent of the target to be detected, a single NHP can be used for the detection of any target of interest. Fourth, CLD is directly prepared from loop-mediated isothermal amplification (LAMP), a simple, cost-effective, widely used nucleic acid amplification technique (Figure S1).[18,19] CLD offers multivalency for ssDNA hybridization, which guarantees high-efficiency NHP blockage in the absence of the target of interest.

In this work we demonstrate the versatility of CLIPON by applying it for detection of three specific targets: human papilloma virus (HPV) DNA, genomic RNA from SARS-CoV-2 and adenosine (a non-nucleic acid target). By coupling recombinase polymerase amplification (RPA) as an upstream amplifier, CLIPON is able to achieve a detection sensitivity at single-copy range (≈aM). A mobile phone imaging app and a hand-held microfluidic device are also developed to further enhance the user-friendliness of CLIPON.

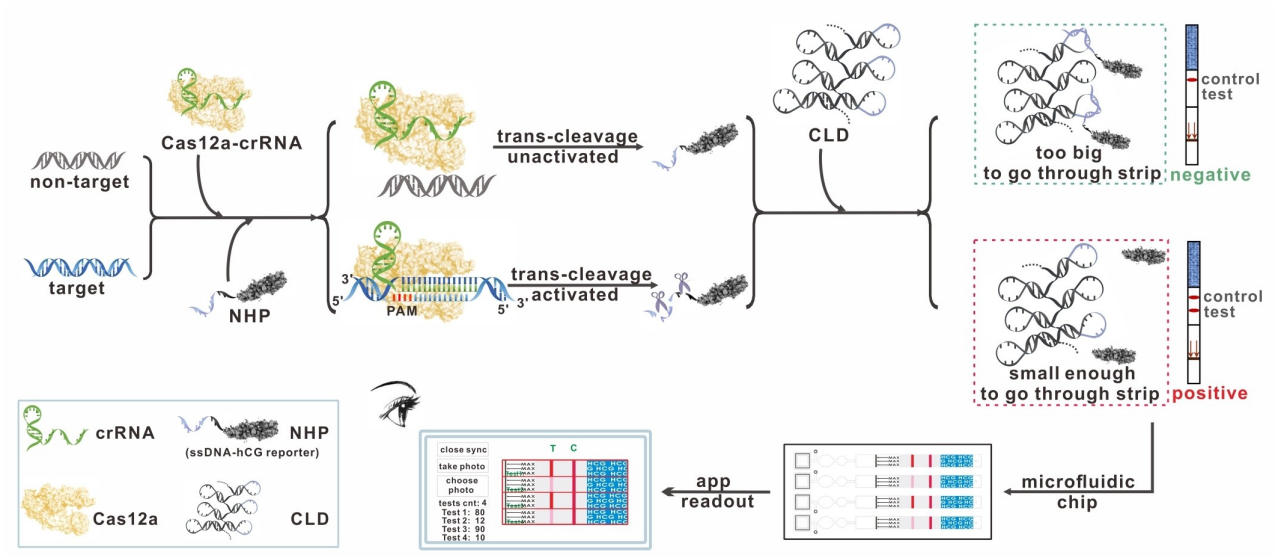


Figure 1. Illustration of CLIPON using the detection of a double-stranded DNA target as the target of interest.

© 2022 Wiley-VCH GmbH

15213773, 2022, 12, Downloaded from https://onlinelibrary.wiley.com/doi/10.1002/anie.202115907 by Shanghai Normal University, Wiley Online Library on [05/02/2023]. See the Terms and Conditions (https://onlinelibrary.wiley.com/terms-and-conditions) on Wiley Online Library for rules of use; OA articles are governed by the applicable Creative Commons License

Results and Discussion

Initial Validation of CLIPON with a Synthetic Double-Stranded DNA

As shown in Figure 1, the CLIPON transduces the presence of a nucleic acid target to a colorimetric readout on PTS through: 1) the hybridization between NHP and CLD that makes hCG unavailable for migrating on PTS and 2) cleavage of the DNA tag within NHP by Cas12a upon target-crRNA binding, which releases hCG from NHP for migration on PTS. As the first step of validating CLIPON, we used a simple dsDNA target, named dsDNA-T1, representing a DNA fragment within HPV-16-L1 gene.

A fluorescence assay was designed to assess the trans DNA cleavage activity of Cas12a-crRNA.[12,20] LbCas12a, which has been shown to exhibit higher trans DNA cleavage activity than the AsCas12a or the FnCas12a,[21,22] was chosen for this work. The crRNA was designed to be complementary of dsDNA-T1. A 15-nt AT-rich fluorescent DNA probe named FQDNA1 (5′-FAM-TTATTTTATTTTATT-quencher-3′) was used to assess the trans cleavage activity of LbCas12a, which is known to preferentially cleave AT-rich sequences.[21] In presence of both dsDNA-T1 and LbCas12a-crRNA, FQDNA1 is expected to be cleaved and produce an enhanced fluorescence signal. Indeed, fluorescence was observed to increase as a function of the concentration of dsDNA-T1 when FQDNA1 was incubated with LbCas12a-crRNA and dsDNA-T1 (Figure 2a). For example, at 0.5 nM dsDNA-T1, it took 40 min for the system to reach maximal fluorescence, but at 5 nM dsDNA-T1, the system only needed less than 10 min to reach the plateau. In contrast, no fluorescence increase was detected when dsDNA-T1 was completely absent.

The CLD was prepared by LAMP (Figure S1) using a dsDNA named Template 1 as the DNA template.[4,7] As shown by agarose gel electrophoresis (Figure S2a and S2c), the LAMP reaction is very efficient. The main CLD was trapped at the loading well, indicating a size that is significantly larger than the 10 kilobase dsDNA marker used for the gel electrophoresis experiment. The DNA tag in NHP is named ssDNA1, which is 29-nt long and was designed to contain two sequence segments (Figure 2b): a 14-nt segment (shown in red) that is complementary to the

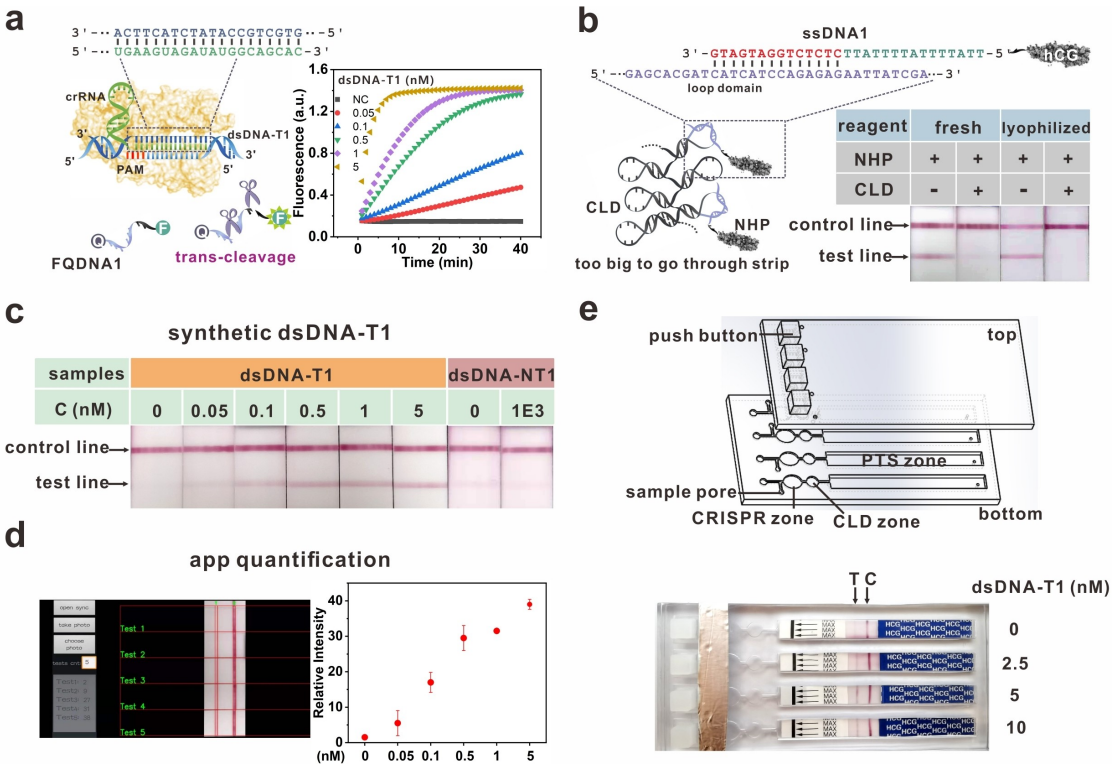


Figure 2. Validation of CLIPON using a synthetic dsDNA target, dsDNA-T1. a) Fluorescence assay that verifies the cleavage activity of LbCas12a upon crRNA-dsDNA-T1 binding. Left panel: graphic illustration of the binding and cleavage reactions involving dsDNA-T1, FQDNA1, LbCas12a and crRNA. Right panel: Fluorescence profiling of the binding and cleavage reactions with increasing concentrations of dsDNA-T1. b) Blockage of migration of NHP on PTS by CLD. The hybridization involving the loop sequence of CLD and the ssDNA1 tag of NHP is shown on the top left. "−" and "+": the image of PTS with NHP only and with NHP plus CLD, respectively. c) Signal responses of PTS to increasing concentrations of dsDNA-T1. dsDNA-NT1: control target (that crRNA does not bind) at very high concentration (1000 nM). d) Color quantitation using a mobile app (CLIPON color indicator). Left panel: The user interface of CLIPON color indicator which can quantify five test lines at once. Right panel: Color intensity quantitation for the experiment conducted in panel c. e) Four-channel CLIPON microfluidic chip. Top portion: schematic illustration of the microfluidic chip; bottom portion: the PTS responses to four different concentrations of dsDNA-T1. The error bars represent standard deviation from two independent tests.

© 2022 Wiley-VCH GmbH

15213773, 2022, 12, Downloaded from https://onlinelibrary.wiley.com/doi/10.1002/anie.202115907 by Shanghai Normal University, Wiley Online Library on [05/02/2023]. See the Terms and Conditions (https://onlinelibrary.wiley.com/terms-and-conditions) on Wiley Online Library for rules of use; OA articles are governed by the applicable Creative Commons License

loop sequence within CLD (so that NHP can bind CLD) and a 15-nt AT-rich sequence (shown in green, which has the identical sequence of FQDNA1) that can be efficiently cleaved by LbCas12a. NHP was prepared from amine-functioned ssDNA1 and SNAP-tagged hCG according to a published protocol (Figure S2b).[7] The conjugation reaction was set up to ensure that the molecular ratio of ssDNA1 to hCG was 1:1. We confirmed the NHP-capturing ability of CLD using agarose gel electrophoresis (Figure S2c). In addition, mixing CLD with NHP indeed blocked the migration of NHP on PTS (Figure 2b), as revealed by disappearance of the test line (the PTS strips marked with "+" for CLD) in comparison to the strong test line when NHP was used alone (the PTS strips marked with "−" for CLD). Note that both NHP and CLD could be freeze-dried for long-term storage, and thus-prepared NHP and CLD showed similar performance with the freshly made materials (labeled with "lyophilized" and "fresh", respectively, in Figure 2b).

Next, we implemented the CLIPON detection of dsDNA-T1 following the steps of NHP cleavage, CLD blockage and PTS signal generation. A standard protocol was established (shown in the experimental section) after several critical parameters affecting the signal-to-background ratio were optimized, which included the cleavage time of LbCas12a-crRNA, reaction buffer components and the concentration of NHP (Figure S3). The PTS responses for different concentrations of dsDNA-T1 are shown in Figure 2c. As expected, the strip with the non-target control did not produce a test line; however, dsDNA-T1 at as low as 50 pM was able to produce a visible test line. The color of the test line intensified when the concentration of dsDNA-T1 was progressively increased. In stark contrast, replacing dsDNA-T1 with a nonspecific target (named dsDNA-NT1) at a very high concentration (1000 nM) produced only a very faint test line that was similar to the one seen with the buffer-only control, demonstrating that the signal production on PTS is target-specific.

We also developed a mobile phone app (named "CLIPON image indicator") to quantify color intensity of PTS, which was set up to calculate the relative intensity by $I_T/I_C \times 100$ where I_T and I_C represents the color intensity of test line and control line of the same strip, respectively. CLIPON image indicator was designed to be user-friendly; by simply entering the number of test samples and aligning the control line and test line into the frame, the $I_T/I_C \times 100$ value of each PTS will be calculated and displayed (Figure 2d left). As an example, the relative color intensity of the PTSs in response to increasing concentration of dsDNA-T1 that were read by the app are shown in the right panel of Figure 2d. We also designed a hand-held microfluidic chip to further simplify on-site testing. As shown in Figure 2e (top portion), the chip was engineered with a capability of simultaneously testing four samples. It is composed of two modules: the top part consists of push buttons for injecting all the reaction reagents to the test strip, and the bottom part comprises of four parallel microfluidic channels to allow four reactions to be performed at the same time. Each microfluidic channel includes four zones: sample pore for loading a test sample, CRISPR reaction zone to allow for LbCas12a-crRNA mediated NHP cleavage in the presence of the target, CLD reaction zone to allow for CLD/NHP hybridization in the absence of the target, and PTS zone for signal generation. Detailed chip operation can be found in the experimental section (SB.2). A miniature heating table (room temperature to 95 °C) is also incorporated to allow the precise control of temperature for each step (Figure S4). The results of simultaneous detection of four different concentrations of dsDNA-T1 are also provided in Figure 2e (bottom portion).

CLIPON for DNA Detection Using Clinical Virus Samples

Having confirmed the function and basic property of the CLIPON platform using dsDNA-T1, we sought to apply the platform for DNA detection using real-world samples. The CLIPON platform is suitable for detection of any dsDNA and ssDNA as long as a specific crRNA is designed with a complementary sequence to the DNA target. As shown in Figure 2, CLIPON can achieve a limit of detection (LOD) of 50 pM without signal amplification. However, in many scenarios it is more desirable to achieve a significantly better LOD (fM–aM). That can be done using isothermal DNA amplification reactions, which have been shown to deliver very low LODs.[12,14,19,23–29] Although there are many choices of isothermal DNA amplification methods, we chose recombinase polymerase amplification (RPA, Figure S5)[30] in this work due to its high amplification efficiency but lack of simple and reliable signal transduction methods. The working mechanism of RPA-CLIPON is illustrated in Figure 3a using the detection of 131-bp HPV-16 gene segment (named dsDNA-HPV16).[12] The target sequence and its relationships to RPA primers and crRNA are presented in Figure 3b. Note that the sequence of crRNA binding site is identical to dsDNA-T1 used in Figure 2, and because of this, all the experimental components and conditions optimized for dsDNA-T1 detection can be directly adapted for the detection of the products of the RPA.

The fluorescence-based cleavage assay (Figure S6) suggests that the 30 min RPA reaction was enough to generate detectable amount of products from as low as 2 copies μL^{-1} dsDNA-HPV16. Therefore, we selected the products of 30 min RPA reaction as the input for CLIPON. The PTS images shown in Figure 3c indicate that RPA-CLIPON can consistently identify dsDNA-HPV16 at 2 copies μL^{-1}, which is consistent with the results obtained with fluorescence-based assay (Figure S6). The concentration of 2 copies μL^{-1} is equivalent to 3.3 aM, which is also consistent with a previously reported CRISPR-based detection method.[12]

Next, we tested whether PRA-CLIPON could be applied for the detection of DNA from real clinical samples. We collected vaginal or urethral discharges from six patients, two were negative (DN1 and DN2) four were positive (DP1-4) with HPV-16. Viral DNA was extracted from these samples using a standard DNA extraction protocol. We first conducted fluorescence-based assays with these samples and the results shown in Figure 3d indicate that RPA-LbCas12a

© 2022 Wiley-VCH GmbH

15213773, 2022, 12, Downloaded from https://onlinelibrary.wiley.com/doi/10.1002/anie.202115907 by Shanghai Normal University, Wiley Online Library on [05/02/2023]. See the Terms and Conditions (https://onlinelibrary.wiley.com/terms-and-conditions) on Wiley Online Library for rules of use; OA articles are governed by the applicable Creative Commons License

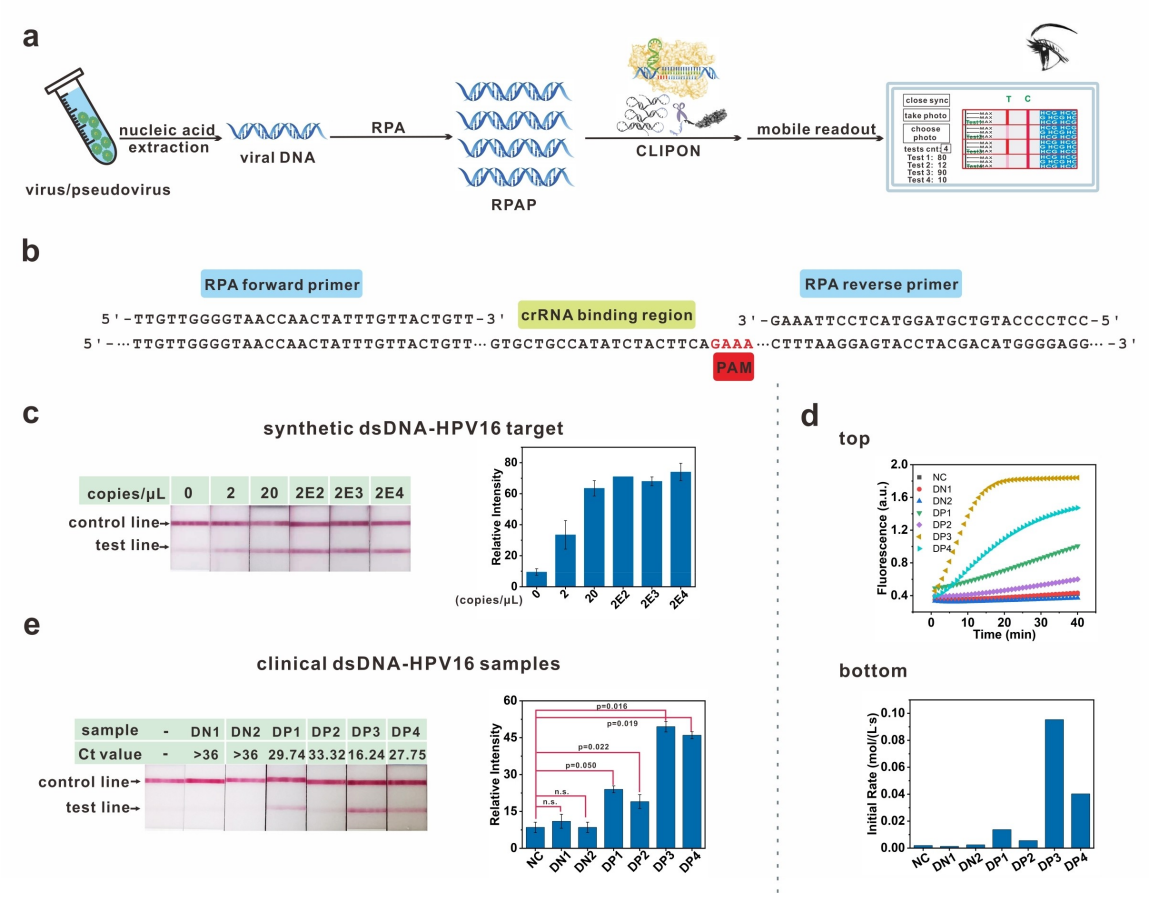


Figure 3. RPA-CLIPON: Coupling CLIPON with recombinase polymerase amplification (RPA) for highly sensitive detection of genomic DNA. a) The working mechanism of RPA-CLIPON. b) The sequence of dsDNA-HPV16 (within HPV-16 gene) and its relationship to RPA primers and crRNA. c) Signal responses of PTS to different amounts of synthetic dsDNA-HPV16 following RPA-CLIPON. Left panel: Photographs of a series of PTSs in response of increasing concentrations of dsDNA-HPV16. Right panel: Color intensity quantification for PTS photographs in left panel. The RPA-CLIPON protocol is the same as that for dsDNA-T1 except that 2 μL of 30 min products of the RPA reaction (Figure S3d) were used. d) Top: The fluorescence-based cleavage assay with 7 samples: water control (NC), and DNA extracts of two HPV-16 negative samples (DN1 and DN2) and four HPV-16 positive (DP1 to DP4) clinical samples. The "DN1 and DN2" were defined as negative sample according to qPCR test, showing a Ct value >36. Bottom: Quantification using the initial fluorescence enhancement rate as the signal. The fluorescence assay works the same way as that of Figure 2a, expect for replacing the dsDNA-T1 with the RPA products (RPAP). e) Signal responses of PTS in the RPA-CLIPON assay to the same set of samples used in panel 3d. Left: photographs of PTS along with Ct values from qPCR analysis. Right: Color intensity quantification for PTS photographs. Statistics analysis was performed using a two-tailed Student t-test, where n.s. = not significant with $p>0.05$.

was able to produce much higher signals with DP1-4 than with DN1 and DN2. We then carried out RPA-CLIPON assays with this set of samples and the results are provided in Figure 3e. The four HPV-16 positive samples all produced a visible test line, and importantly, their color intensities were expectedly found to inversely proportional to the Ct values of qPCR conducted with the same samples (the Ct values are provided in the left panel of Figure 3e). In contrast, the two HPV-16 negative samples produced very weak test lines that were similar to that observed for the negative control (NC: water only). These results show that RPA-CLIPON was capable of detection of HPV-16 from clinical samples.

CLIPON for the Detection of Genomic RNA from SARS-CoV-2

The detection of the genomic RNA from SARS-CoV-2 was investigated next, following a similar procedure shown in Figure 3a. RPA reactions were designed to target a 172-nt segment within the ORF1ab gene of SARS-CoV-2 based on the sequence published on GenBank (MZ146316.1). The key sequence elements of this RNA target and the sequences of the two RPA primers are shown in Figure 4a. First, a synthetic dsDNA sequence (named dsDNA-SARS-CoV-2) was used to establish reaction conditions. Note that we chose this RNA segment for detection as it is conserved in the wide-type virus and most of the current variants of concern. The results from gel electrophoresis and fluorescence cleavage assays verified the DNA amplification by RPA, the recognition of the RPAP by crRNA and the trans cleavage activity of LbCas12a (Figures S7 and S8). The

© 2022 Wiley-VCH GmbH

15213773, 2022, 12, Downloaded from https://onlinelibrary.wiley.com/doi/10.1002/anie.202115907 by Shanghai Normal University, Wiley Online Library on [05/02/2023]. See the Terms and Conditions (https://onlinelibrary.wiley.com/terms-and-conditions) on Wiley Online Library for rules of use; OA articles are governed by the applicable Creative Commons License

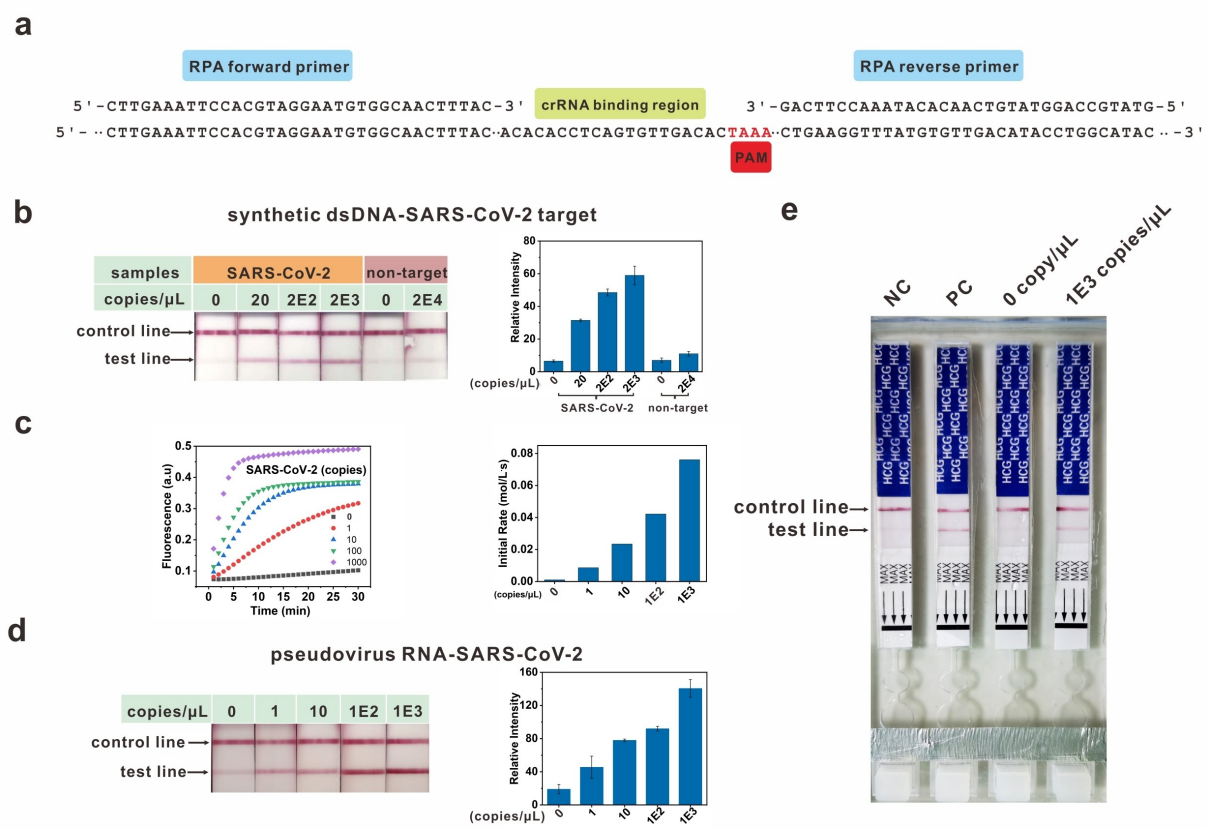


Figure 4. RPA-CLIPON for RNA-SARS-CoV-2 detection. a) The sequence of dsDNA-SARS-CoV-2 (within ORF1ab gene) and its relationship to RPA primers and crRNA. b) Signal responses of PTS to different amounts of synthetic dsDNA-SARS-CoV-2 following RPA-CLIPON. Left panel: Photographs of a series of PTSs in response to increasing concentrations of dsDNA-SARS-CoV-2. Right Panel: Color intensity quantification for PTS photographs in the left panel. Non-target controls are mixtures of RPAP from 0 and 2000 (2E3) copies μL^{-1} dsDNA-HPV16. c) Left: The fluorescence-based cleavage assay for RT-RPAP from different amounts of RNA-SARS-CoV-2 exacted from pseudovirus. Right: Quantification using the initial fluorescence increase rate. The assay works the same way as that shown in Figure 2a, except for replacing dsDNA-T1 with the RPAP. d) Signal responses of PTS (after RT-RPA-CLIPON detection) to different amounts of RNA-SARS-CoV-2 extracted from pseudovirus. Left panel: Signal responses of PTS. Right Panel: Color intensity quantitation for PTS photographs in the left panel. The RT-RPA-CLIPON was conducted in the same way as that for dsDNA-T1 except that 2 μL RT-RPAP after 30 min RT-RPA reaction was used as the input (to replace dsDNA-T1). e) The microfluidic chip based assay with negative and positive SARS-CoV-2 pseudovirus samples. NC and PC: the RPAP produced from 0 and 2000 copies μL^{-1} synthetic dsDNA-HPV16. The "0 copy μL^{-1}" and "1E3 copies μL^{-1}" represent the RPAP produced from 0 copy μL^{-1} and 1000 copies μL^{-1} RNA-SARS-CoV-2 extracted from pseudovirus.

image provided in Figure 4b demonstrates that the RPA-COLIPON was able to detect low amounts of dsDNA-SARS-CoV-2, as the three dsDNA-SARS-CoV-2 samples produced strong test lines while the non-target control (the RPAP produced from 2000 copies of dsDNA-HPV16 with its primer set used for HPV-16) generated a very weak test line that was similar to the water control (labeled "0"). These results show that the designed RPA-CLIPON-SARS-CoV-2 system was able to detect dsDNA-SARS-CoV-2 specifically and at low levels (20 copies μL^{-1}).

We then applied the RPA-CLIPON-SARS-CoV-2 system for the detection of genomic RNA of SARS-CoV-2 (named RNA-SARS-CoV-2). RPA reaction was replaced by one-step reverse transcription RPA (RT-RPA) for RNA detection. Due to very limited access to real SARS-CoV-2 samples in China, pseudovirus with same virus structure but no infectivity was used for this experiment. Following viral RNA extraction and RT-PRA, both fluorescence-based cleavage assay (Figure 4c) and the CLIPON assay (Figure 4d) were performed, both of which were found to be able to detect RNA-SARS-CoV-2 at 1000 copy mL^{-1} (equivalent to 1.6 aM). This detection sensitivity is adequate for COVID-19 detection with clinical samples. It is noteworthy that the sensitivity of RNA detection is higher than that of DNA detection due to the additional amplification from reverse transcription. The RT-RPA-CLIPON platform can consistently detect SARS-CoV-2 pseudovirus RNA at 1 copy μL^{-1} but produced inconsistent results at lower concentrations. We further validated the detection of RNA-SARS-CoV-2 using the microfluidic setup (Figure 4e; RPAP produced with 2000 copies μL^{-1} dsDNA-HPV16 were used as the positive control, which is marked with PC; NC: water).

© 2022 Wiley-VCH GmbH

15213773, 2022, 12, Downloaded from https://onlinelibrary.wiley.com/doi/10.1002/anie.202115907 by Shanghai Normal University, Wiley Online Library on [05/02/2023]. See the Terms and Conditions (https://onlinelibrary.wiley.com/terms-and-conditions) on Wiley Online Library for rules of use; OA articles are governed by the applicable Creative Commons License

CLIPON for the Detection of Non-Nucleic Acid Targets

Finally, we expanded the utility of CLIPON for the detection of a non-nucleic acid target via integration of LbCas12a-crRNA with an aptamer as the recognition element (Aptamer-CLIPON).[31,32] Herein, the aptamer is designed to be part of a Duplex Switch made of two different DNA molecules denoted "probe 1" and "probe 2" (Figure 5a). Probe 1 contains both the aptamer element (red sequence) and non-aptamer element (grey sequence). The non-aptamer element and part of the aptamer element are designed to be complementary to part of probe 2 so that a strong duplex is created between probe 1 and probe 2. Importantly, the formation of this strong duplex prevents easy access to the sequence element (blue sequence) within probe 2 by the crRNA. As a result, the trans cleavage activity of LbCas12a cannot be activated. In the presence of the cognate target for the aptamer, probe 1 chooses to form the aptamer-target complex, making the blue sequence more accessible by the crRNA. Consequently, the CRISPR complex is activated for its trans cleavage activity. In other words, the non-aptamer element and part of the aptamer element of probe 1 function as the blocker for the access of the complementary sequence of probe 2 by the LbCas12a-crRNA complex and the formation of the aptamer-target complex removes this blockage. The star advantage of this Duplex Switch over previous design[16] is the aptamer sequence is non-relevant to that of activator. So the Duplex Switch can be, theoretically, applied to any target merely by changing aptamer sequence.

A well-studied structure-switching DNA aptamer that responds to adenosine was used as the model aptamer to validate the proposed idea.[16,33,34] The sequences of probe 1, probe 2 and the Duplex Switch is shown in Figure 5b. The recognition sequence of crRNA in this system is a ssDNA (blue sequence) rather than the dsDNA used in previous systems, and therefore we optimized the trans cleavage efficiency of the system (Figure S9). A fluorescence-based cleavage assay was performed to determine the response of the system to adenosine. As expected, fluorescence intensity increased as a function of rising adenosine concentrations (Figure 5c). The system was found to be highly specific for adenosine as the addition of 800 μM cytosine, guanosine,

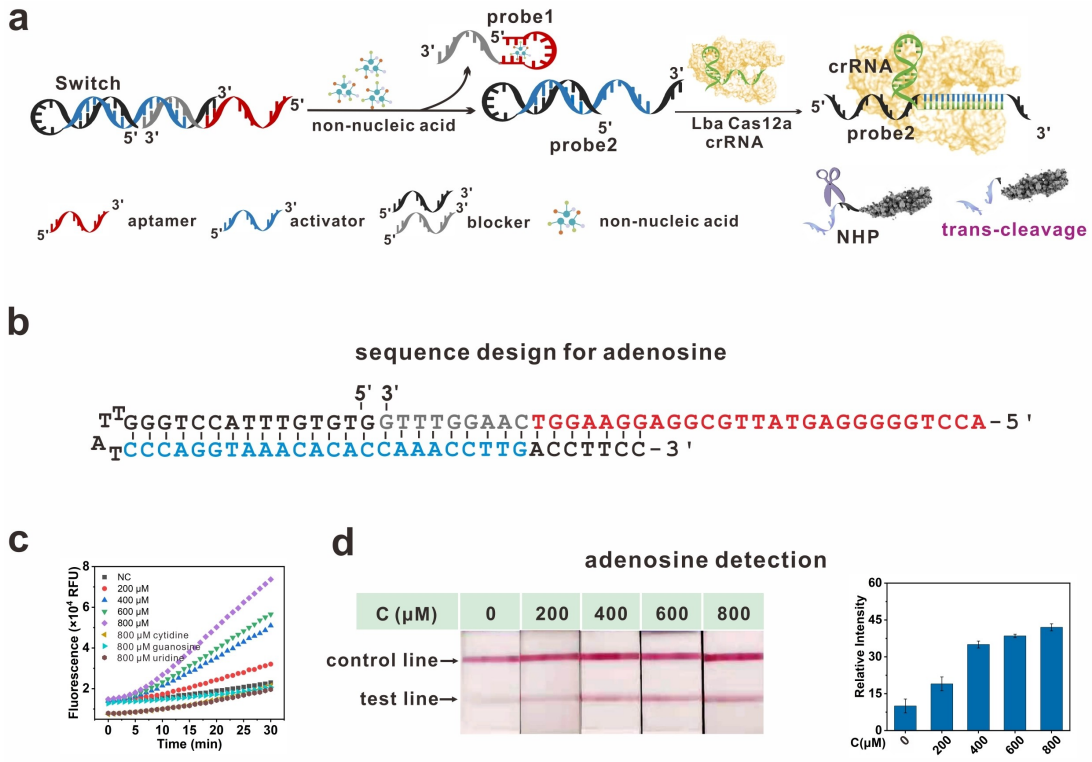


Figure 5. Design of a Duplex Switch to allow the expansion of CLIPON for the detection of non-nucleic acid targets. a) Working principle. A Duplex Switch is made of two DNA molecules, probe 1 and probe 2. Probe 1 contains an aptamer element (red) and a non-aptamer element (grey). Probe 2 is a hairpin that contains the crRNA-binding sequence (blue) and a hairpin structure element (black). Hybridization of probe 1 with probe 2 leads to the formation of the Duplex Switch, which hinders the access of crRNA to its complementary sequence in probe 2. However, this hinderance is removed in the presence of the target for the aptamer due to the formation of the aptamer–target complex. Consequently, the trans cleavage function of LbCas12a-crRNA is activated. Because the aptamer sequence is non-relevant to that of activator, the Duplex Switch can be, theoretically, applied to any target merely by changing aptamer sequence. b) The sequence of the Duplex Switch for adenosine detection. c) The fluorescence-based cleavage assay involving LbCas12a-crRNA, the Duplex Switch for adenosine and FQDNA1. d) CLIPON for the detection of adenosine. Left panel: photographs of PTSs in response to different concentrations of adenosine. Right panel: quantification of the test lines using CLIPON color indicator.

© 2022 Wiley-VCH GmbH

15213773, 2022, 12, Downloaded from https://onlinelibrary.wiley.com/doi/10.1002/anie.202115907 by Shanghai Normal University, Wiley Online Library on [05/02/2023]. See the Terms and Conditions (https://onlinelibrary.wiley.com/terms-and-conditions) on Wiley Online Library for rules of use; OA articles are governed by the applicable Creative Commons License

uridine did not induce significant fluorescence enhancement (Figure 5c).

Subsequently, we integrated the Duplex Switch into the CLIPON system to achieve the visual detection of adenosine using PTS (Figure 5d). Note that the testing protocol was very similar to the one used for the detection of dsDNA-T1 except that dsDNA-T1 was replaced with the Duplex Switch shown in Figure 5b. In addition, the test temperature was set to be 25 °C to minimize the background signal, although LbCas12a has the best enzymatic activity at 37 °C (Figure S10).[35] The cleavage time was kept at 30 min to minimize signal-to-background ratios (longer reaction times was found to produce higher levels of background signal). The data presented in Figure 5d clearly shows that stronger and stronger test lines were produced with the increasing concentration of adenosine. When using longer cleavage time (60 min), this CLIPON system was capable of detecting 50 μM adenosine (Figure S11–S12), which is consistent with a previously described biosensor using the same aptamer.[16]

Conclusion

Herein we rationally integrate commercial pregnancy test strips, CRISPR-Cas12a and a large-sized DNA assembly called CLD into a biosensing platform termed CLIPON (CRISPR and Large DNA assembly Induced Pregnancy Strips Signal-ON Detection). With the use of PTS, which can be purchased through pharmacies or online, CLIPON represents a very simple approach for biosensing and has the potential of being used to set up point-of-care or point-of-need detection methods. CLIPON is versatile and can be configured for the sensitive and specific detection of DNA, RNA and non-nucleic acid targets. With the design of mobile app and a microfluidic chip, CLIPON systems become highly automated and can complete a test in a timely fashion. For example, CLIPON is capable of detection HPV DNA and SARS-CoV-2 RNA down to ≈ aM LOD at a cost per test of 3–7 US dollar (see Supporting Information, SB.3 and Figure S13 for detailed procedure and cost analysis). Currently, only the CLIPON step can be completed on the microfluidic system; sample processing and amplification are carried out as upstream steps. However, because aptamer-target recognitions usually do not require a target isolation step, Duplex Switch-CLIPON can be carried out entirely on the microfluidic system after a simple sample mixing step, and thus is more suitable for applications at the point of need.

Efforts are still required to further improve CLIPON to make it a truly "plug-in" POCT method for nucleic acid testing as our current method still requires upstream sample treatment and amplification. However, there are successful demonstrations that RPA and Cas12a cleavage can be carried out in a single step,[36] and Cas12a cleavage can function well on nano-/micro-surfaces.[15,24,37] Therefore, it is possible to further integrate RPA, NHP cleavage, and CLD blockage into a simple single-step procedure. Meanwhile, further improvement in reagent purity, image acquisition techniques, and data analysis methods are expected to further advance CLIPON into a more reliable quantitative method.

Acknowledgements

We are grateful to Defeng Song in China-Japan Union Hospital of Jilin University for providing the clinical samples. This work is financially supported by National Key Technologies Research and Development Program of China (2019YFC1905400), Natural Science Foundation of China (22004118, 21874129, 22174137), Key Technology Research and Development Program of Jilin Province (20200404178YY, 202102041266YY), Achievement Transformation Project of Bethune First Hospital of Jilin University-Changchun Institute of Applied Chemistry (CGZHYD202012-021), and International Scientific Cooperation Project of Jilin Scientific and Technological Development Program (No. 20200801044GH).

Conflict of Interest

The authors declare no conflict of interest.

Data Availability Statement

The data that support the findings of this study are available from the corresponding author upon reasonable request.

Keywords: CRISPR-Cas12a · Nucleic Acid Detection · Point-of-Care Diagnostic · Pregnancy Strips · SARS-CoV-2

[1] J. Liu, D. Mazumdar, Y. Lu, *Angew. Chem. Int. Ed.* **2006**, *45*, 7955–7959; *Angew. Chem.* **2006**, *118*, 8123–8127.
[2] K. Tram, P. Kanda, B. J. Salena, S. Huan, Y. Li, *Angew. Chem. Int. Ed.* **2014**, *53*, 12799–12802; *Angew. Chem.* **2014**, *126*, 13013–13016.
[3] Y. Xiang, Y. Lu, *Nat. Chem.* **2011**, *3*, 697–703.
[4] Y. Du, R. A. Hughes, S. Bhadra, Y. S. Jiang, A. D. Ellington, B. Li, *Sci. Rep.* **2015**, *5*, 11039.
[5] Y. Tang, H. Li, B. Li, *Chem. Commun.* **2020**, *56*, 2483–2486.
[6] E. Amalfitano, M. Karlikow, M. Norouzi, K. Jaenes, S. Cicek, F. Masum, P. S. Mousavi, Y. Guo, L. Tang, A. Sydor, D. Ma, J. D. Pearson, D. Trcka, M. Pinette, A. Ambagala, S. Babiuk, B. Pickering, J. Wrana, R. Bremner, T. Mazzulli, D. Sinton, J. H. Brumell, A. A. Green, K. Pardee, *Nat. Commun.* **2021**, *12*, 724.
[7] Y. Du, A. Pothukuchy, J. D. Gollihar, A. Nourani, B. Li, A. D. Ellington, *Angew. Chem. Int. Ed.* **2017**, *56*, 992–996; *Angew. Chem.* **2017**, *129*, 1012–1016.
[8] Y. Zhang, C. Ma, M. Yang, A. Pothukuchy, Y. Du, *Sens. Actuators B* **2019**, *288*, 163–170.
[9] L. Qi, M. Yang, D. Chang, W. Zhao, S. Zhang, Y. Du, Y. Li, *Angew. Chem. Int. Ed.* **2021**, *60*, 24823–24827; *Angew. Chem.* **2021**, *133*, 25027–25031.
[10] M. Yang, Y. Tang, L. Qi, S. Zhang, Y. Liu, B. Lu, J. Yu, K. Zhu, B. Li, Y. Du, *Anal. Chem.* **2021**, *93*, 11956–11964.
[11] B. Zetsche, J. S. Gootenberg, O. O. Abudayyeh, I. M. Slaymaker, K. S. Makarova, P. Essletzbichler, S. E. Volz, J. Joung,

© 2022 Wiley-VCH GmbH

15213773, 2022, 12, Downloaded from https://onlinelibrary.wiley.com/doi/10.1002/anie.202115907 by Shanghai Normal University, Wiley Online Library on [05/02/2023]. See the Terms and Conditions (https://onlinelibrary.wiley.com/terms-and-conditions) on Wiley Online Library for rules of use; OA articles are governed by the applicable Creative Commons License

J. van der Oost, A. Regev, E. V. Koonin, F. Zhang, *Cell* **2015**, *163*, 759–771.
[12] J. S. Chen, E. Ma, L. B. Harrington, M. D. Costa, X. Tian, J. M. Palefsky, J. A. Doudn, *Science* **2018**, *360*, 436–439.
[13] J. S. Gootenberg, O. O. Abudayyeh, M. J. Kellner, J. Joung, J. J. Collins, F. Zhang, *Science* **2018**, *360*, 439–444.
[14] J. P. Broughton, X. Deng, G. Yu, C. L. Fasching, V. Servellita, J. Singh, X. Miao, J. A. Streithorst, A. Granados, A. Sotomayor-Gonzalez, K. Zorn, A. Gopez, E. Hsu, W. Gu, S. Miller, C. Y. Pan, H. Guevara, D. A. Wadford, J. S. Chen, C. Y. Chiu, *Nat. Biotechnol.* **2020**, *38*, 870–874.
[15] Y. Dai, R. A. Somoza, L. Wang, J. F. Welter, Y. Li, A. I. Caplan, C. C. Liu, *Angew. Chem. Int. Ed.* **2019**, *58*, 17399–17405; *Angew. Chem.* **2019**, *131*, 17560–17566.
[16] Y. Xiong, J. Zhang, Z. Yang, Q. Mou, Y. Ma, Y. Xiong, Y. Lu, *J. Am. Chem. Soc.* **2020**, *142*, 207–213.
[17] B. Pang, J. Xu, Y. Liu, H. Peng, W. Feng, Y. Cao, J. Wu, H. Xiao, K. Pabbaraju, G. Tipples, M. A. Joyce, H. A. Saffran, D. L. Tyrrell, H. Zhang, X. C. Le, *Anal. Chem.* **2020**, *92*, 16204–16212.
[18] T. Notomi, H. Okayama, H. Masubuchi, T. Yonekawa, K. Watanabe, N. Amino, T. Hase, *Nucleic Acids Res.* **2000**, *28*, e63.
[19] Y. Tang, B. Lu, Z. Zhu, B. Li, *Chem. Sci.* **2018**, *9*, 760–769.
[20] B. Wang, R. Wang, D. Wang, J. Wu, J. Li, J. Wang, H. Liu, Y. Wang, *Anal. Chem.* **2019**, *91*, 12156–12161.
[21] L. T. Nguyen, B. M. Smith, P. K. Jain, *Nat. Commun.* **2020**, *11*, 4906.
[22] R. T. Fuchs, J. Curcuru, M. Mabuchi, P. Yourik, G. B. Robb, *biorxiv* **2019**, Preprint at https://www.biorxiv.org/content/10.1101/600890v1.
[23] K. Pardee, A. A. Green, M. K. Takahashi, D. Braff, G. Lambert, J. W. Lee, T. Ferrante, D. Ma, N. Donghia, M. Fan, N. M. Daringer, I. Bosch, D. M. Dudley, D. H. O'Connor, L. Gehrke, J. J. Collins, *Cell* **2016**, *165*, 1255–1266.
[24] W. S. Zhang, J. Pan, F. Li, M. Zhu, M. Xu, H. Zhu, Y. Yu, G. Su, *Anal. Chem.* **2021**, *93*, 4126–4133.
[25] Y. Zhao, F. Chen, J. Qin, J. Wei, W. Wu, Y. Zhao, *Chem. Sci.* **2018**, *9*, 392–397.
[26] Y. Jiang, B. Li, J. N. Milligan, S. Bhadra, A. D. Ellington, *J. Am. Chem. Soc.* **2013**, *135*, 7430–7433.
[27] H. Wang, C. Li, X. Liu, X. Zhou, F. Wang, *Chem. Sci.* **2018**, *9*, 5842–5849.
[28] B. Li, X. Chen, A. D. Ellington, *Anal. Chem.* **2012**, *84*, 8371–8377.
[29] Y. Kimura, M. J. L. de Hoon, S. Aoki, Y. Ishizu, Y. Kawai, Y. Kogo, C. O. Daub, A. Lezhava, E. Arner, Y. Hayashizaki, *Nucleic Acids Res.* **2011**, *39*, e59.
[30] O. Piepenburg, C. H. Williams, D. L. Stemple, N. A. Armes, *PLoS Biol.* **2006**, *4*, e204.
[31] A. D. Ellington, J. W. Szostak, *Nature* **1990**, *346*, 818–822.
[32] C. Tuerk, L. Gold, *Science* **1990**, *249*, 505–510.
[33] R. Nutiu, Y. Li, *J. Am. Chem. Soc.* **2003**, *125*, 4771–4778.
[34] R. Nutiu, Y. Li, *Angew. Chem. Int. Ed.* **2005**, *44*, 1061–1065; *Angew. Chem.* **2005**, *117*, 1085–1089.
[35] K. H. Ooi, M. M. Liu, J. W. D. Tay, S. Y. Teo, P. Kaewsapsak, S. Jin, C. K. Lee, J. Hou, S. Maurer-Stroh, W. Lin, B. Yan, G. Yan, Y. G. Gao, M. H. Tan, *Nat. Commun.* **2021**, *12*, 1739.
[36] W. Feng, H. Peng, J. Xu, Y. Liu, K. Pabbaraju, G. Tipples, M. A. Joyce, H. A. Saffran, D. L. Tyrrell, S. Babiuk, H. Zhang, X. C. Le, *Anal. Chem.* **2021**, *93*, 12808–12816.
[37] R. Liu, Y. Hu, Y. He, T. Lan, J. Zhang, *Chem. Sci.* **2021**, *12*, 9022–9030.

Manuscript received: November 22, 2021
Accepted manuscript online: January 22, 2022
Version of record online: February 2, 2022

© 2022 Wiley-VCH GmbH

15213773, 2022, 12, Downloaded from https://onlinelibrary.wiley.com/doi/10.1002/anie.202115907 by Shanghai Normal University, Wiley Online Library on [05/02/2023]. See the Terms and Conditions (https://onlinelibrary.wiley.com/terms-and-conditions) on Wiley Online Library for rules of use; OA articles are governed by the applicable Creative Commons License